OATAO

Open Archive Toulouse Archive Ouverte

Open Archive Toulouse Archive Ouverte (OATAO)

OATAO is an open access repository that collects the work of Toulouse researchers and makes it freely available over the web where possible.

Experimental and numerical study of the accuracy of flame-speed measurements for methane/air combustion in a slot burner

L. Selle [a,b,*], T. Poinsot [a,b,c], B. Ferret [a,b]

[a] *Université de Toulouse, INPT, UPS, IMFT (Institut de Mécanique des Fluides de Toulouse), Allée Camille Soula, F-31400 Toulouse, France*
[b] *CNRS, IMFT, F-31400 Toulouse, France*
[c] *CERFACS, 42 Av. G. Coriolis, 31057 Toulouse cedex, France*

ABSTRACT

Measuring the velocities of premixed laminar flames with precision remains a controversial issue in the combustion community. This paper studies the accuracy of such measurements in two-dimensional slot burners and shows that while methane/air flame speeds can be measured with reasonable accuracy, the method may lack precision for other mixtures such as hydrogen/air. Curvature at the flame tip, strain on the flame sides and local quenching at the flame base can modify local flame speeds and require corrections which are studied using two-dimensional DNS. Numerical simulations also provide stretch, displacement and consumption flame speeds along the flame front. For methane/air flames, DNS show that the local stretch remains small so that the local consumption speed is very close to the unstretched premixed flame speed. The only correction needed to correctly predict flame speeds in this case is due to the finite aspect ratio of the slot used to inject the premixed gases which induces a flow acceleration in the measurement region (this correction can be evaluated from velocity measurement in the slot section or from an analytical solution). The method is applied to methane/air flames with and without water addition and results are compared to experimental data found in the literature. The paper then discusses the limitations of the slot-burner method to measure flame speeds for other mixtures and shows that it is not well adapted to mixtures with a Lewis number far from unity, such as hydrogen/air flames.

1. Introduction

Determining the laminar flame speed of premixed flames is one of the oldest problem in combustion [1–4]. It is not only an academic problem limited to laminar flames: in most models for turbulent combustion systems [5–8], the laminar premixed flame speed is an essential ingredient, either to validate the chemical scheme used in the source terms (in pdf methods [9] for example) or to provide the speed of the flamelets (in the *G* equation formulation [6] or in the Coherent Flame model [10] for example). Measuring or calculating laminar flame speeds [1,11–13] however remains a difficult challenge. Multiple methods can be used to measure laminar flame speeds: (1) the propagating flame in a tube, (2) the stagnation-point flame, (3) the spherical unsteady flame, (4) the heat-flux method and (5) the slot burner.

For all methods, it is possible to use either an experiment or a simulation. Method 1 seems simple: measuring the position vs. time of a laminar flame propagating in a tube gives a flame speed [2–4]. Method 2 uses a stagnation-point flow configuration [14–16] where the flame is stabilized in a counter flow and velocity measurements are used to deduce the displacement speed of the front relative to the flow. In Method 3 a spherical deflagration is created by igniting a premixed stagnant flow and measuring the pressure vs. time [4,17,18] or in more recent techniques, the position of the flame front vs. time [19–21]. This absolute flame speed must be corrected by the density ratio of burnt to fresh gases to provide the laminar flame speed. This technique is commonly used and works at high pressures [22] as well as for turbulent flames [23–25]. The heat-flux method (4) is not recent [26] but has lately been receiving increasing attention [27,28] because it produces a flat stretch-free flame. Method 5 (the slot burner) is the topic of this paper and has been used for more than a century [1,29,30]. In this method a simple measurement of the height or of the surface of a flame stabilized over an orifice is sufficient to evaluate the flame speed.

All methods to measure flame speeds have drawbacks: Method 1 requires planar propagating flames but producing such flames in the absence of any instability or wall effects is difficult [31,32] and this method, which works well for detonations, is not often used for deflagrations. Method 2 requires to measure the velocity field in a complex stagnation-point flow where the flow velocity is

* Corresponding author at: Université de Toulouse, INPT, UPS, IMFT (Institut de Mécanique des Fluides de Toulouse), Allée Camille Soula, F-31400 Toulouse, France. Fax: +33 534 32 29 94.

E-mail address: laurent.selle@imft.fr (L. Selle).

strongly varying and sophisticated interpolation methods are needed to find the flow speed at the flame location and deduce a flame speed. Moreover, the stagnation-point flame is stretched and a model for the effects of stretch on flame speed is required to extrapolate the flame speed at zero stretch. The same problem arises in Method 3 where the spherical flame is obviously growing and therefore stretched. Moreover, the precision of flame-speed measurements in spherical flames is the source of multiple controversies [20,33] because the front may not remain perfectly spherical and is continuously submitted to a varying stretch [34–36]. One great advantage of method 4 is that it does not require a model for stretch or curvature effects on the flame speed. Its accuracy basically depends on the precision of temperature measurements.

The slot-burner technique of Method 5 is probably the simplest one and this paper focuses on its capacities and limitations. First, methane/air flames stabilized on a slot burner are studied using three approaches:

- an experimental measurement in the slot-burner set-up (using two methods to evaluate the flame length),
- a numerical calculation in a one-dimensional configuration using COSILAB and a full scheme for methane (GRI-Mech 3.0 [37]) which gives a flame speed called $s_L^0(GRI)$ and
- a two-dimensional calculation of the exact experimental set-up using a Direct Numerical Simulation (DNS) code [38,39] and a simplified two-step chemical scheme (called 2SCM2) used in previous LES studies [40]. The same code is also used to compute the laminar flame speed $s_L^0(2SCM2)$ for a one-dimensional flame with 2SCM2 to be used as a reference for two-dimensional cases.

Using these three methods together allows to quantify the systematic errors associated with the measurement of methane/air flame speeds using the length of a flame stabilized on a two-dimensional slot. In Section 2 the experimental set-up is presented; then the methodology and potential sources of errors are discussed in Section 3. Section 4 presents the numerical tools: 1D code for flames (COSILAB) and two-dimensional DNS code. The results are described first by investigating the flame structure revealed by DNS (Section 5), then evaluating systematic measurement errors using DNS data (Section 6) and comparing the experimental results with the COSILAB data and literature results (Section 7). All tests are performed for a methane/air flame at atmospheric pressure (1 bar) and standard temperature (300 K) over a range of equivalence ratio ϕ, going from 0.8 to 1.2 (Section 7.1). To illustrate the potential of the method, it is finally used in Section 7.2 to study the influence of water vapor addition on flame speed for a stoichiometric flame. The last part of

the paper (Section 8) discusses the limitations of the slot-burner method. Numerous effects (buoyancy, instabilities, non-unity Lewis number, etc.) that may impact the precision of the measurement are discussed to try and define the type of flames for which the slot-burner technique may be a good choice for flame-speed measurements. A DNS of hydrogen/air flames is used to demonstrate that the slot-burner method is difficult to apply for mixtures having a Lewis numbers far from unity.

The setup chosen here is a rectangular slot rather than circular as often found in the literature. The reasons for this are twofold: (1) in this 2D slot burner, the flame sheets are perfectly planar in the measurement area and no curvature effect has to be taken into account (except at the flame tip unlike in the axisymmetric case where all flame sheets are curved) [29,30] and (2) simulations are easier as well as velocity measurements.

2. Experimental set-up

The experiment used to measure the flame speed of a methane/air mixture is presented in Fig. 1. Flow rates are controlled and measured using Bronkhorst flow meters. The temperature is regulated to ensure a constant value in the plenum. Air is injected tangentially in the plenum where it mixes with methane jets. The flow is then laminarized by an array of small balls, a honeycomb section and a converging nozzle. The slot used to stabilize the flame is $h = 10$ mm wide and $L = 100$ mm long. The slot is water cooled and its surface temperature was measured around 350 K.

Example of flames observed along the y axis are given in Fig. 2 for an equivalence ratio ϕ of 0.8 (left) and 1 (right). The flame is thin, its length is easy to measure and changes strongly when ϕ varies making flame-speed measurements straightforward. A small quenched zone is observed at the flame base while its tip exhibits significant curvature: these effects are quantified in Section 5. A view of the flame along the x axis is presented in Fig. 3 for $\phi = 0.8$: all measurements are performed in the central part of the slot (rectangular box of Fig. 3), where the flame is almost perfectly two-dimensional. The side effects on the flame shape at $y = 0$ and $y = L$ are discussed in Section 6.

To illustrate the method used to measure the flame length, a typical image of the flame obtained for a bulk velocity U_b of 1.7 m/s and an equivalence ratio ϕ of 0.8 is given in Fig. 4. This image is used to evaluate the flame length L_f using two methods. In the first one (TRIANG), the flame is assumed to be a perfect triangle and its length L_f is evaluated as $L_f^T = 2x$ where x is the triangle side length. In the second method (IMAGE), the line corresponding to the maximum reaction rate is extracted from the flame image (Fig. 4) and its length L_f^I is measured using image analysis.
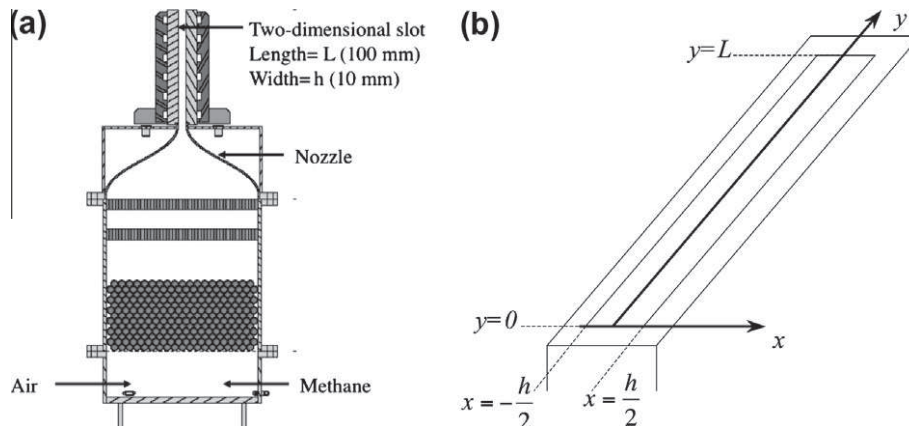

Fig. 1. Slot burner with a square cross section for methane/air flames: (a) cross section of the whole burner, (b) zoom on the outlet section where the flame is stabilized.
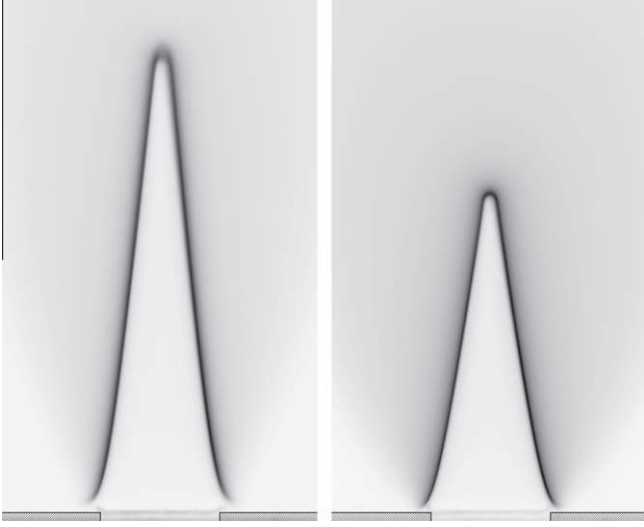
Fig. 2. Flames stabilized on the slot: picture of the experiment. Transverse views at $y = L/2$ for $\phi = 0.8$ (left) and 1.0 (right).

Fig. 3. Side view of the flame (photo of the experiment at $\phi = 0.8$). The rectangular box corresponds to the zone where the measurements of flame length are performed.

3. Principle of method and analysis of systematic errors

The slot burner was one of the first methods used to measure flame speeds [41–43] and experimentalists found out rather soon that it could lead to significant error bars. In particular, one of the early methodologies assumed that the gas velocity profile

was uniform at the outlet of the slot so that the flame angle could be directly related to the flame speed. This approximation is rarely valid and a different approach is used here. Consider the central section of the flame (i.e. $y = L/2$) where the flow is 2D: the integrated consumption of the flame ($\rho Y_F \bar{s}_L L_f$) balances the fresh gases flow rate ($\rho Y_F U h$) so that the mean consumption speed $\bar{s}_L$ averaged along the flame length is given by:

$$\bar{s}_L = \frac{Uh}{L_f} \tag{1}$$

where h is the slot width, U the 2D bulk velocity ($U = 1/h * \int_{-h/2}^{h/2} U(x, y = L/2)dx$) and L_f the flame length, measured either by the TRIANG $\left(L_f^T\right)$ or IMAGE method $\left(L_f^I\right)$. This equation is exact but it does not mean that $\bar{s}_L$ is an exact measurement of the unstretched laminar flame speed s_L^0 at the same pressure, temperature and equivalence ratio: the flame front in the slot-burner configuration may be, in many places, different from an unstretched flame so that its average flame speed $\bar{s}_L$ may differ from s_L^0. Phenomena which can induce such local effects and lead to values of $\bar{s}_L$ which differ from s_L^0 are (a) the quenched region at the flame base near the lips of the slot, (b) strain effects on the flame side which modify locally the flame speed and (c) flame curvature at the flame tip. A second source of error is three-dimensional effects: flame speeds are measured near the center of the slot (Fig. 3) but at this location the 2D bulk velocity $U = 1/h * \int_{-h/2}^{h/2} U(x, y = L/2)dx$ is slightly larger than the mean velocity $U_b = 1/(Lh) * \int_{-h/2}^{h/2} \int_0^L U(x, y)dxdy$ averaged over the whole slot section because the flow is slowed down at each extremity ($y = 0$ and $y = L$) of the slot. Only U_b is measured in the experiment (using a mass-flow meter) so that a model is needed to derive U from U_b.

Because of the large density ratio between the ambient air and the burnt gases, the flame stabilized on a slot burner could be influenced by buoyancy effects [44,45]. The ratio of buoyant to advective forces is the Richardson number Ri = gl/u^2, where g is the acceleration due to gravity, l a characteristic length scale and u the velocity. For our flame Ri $\sim 10^{-2}$ so that it is *a priori* unlikely to be buoyancy driven. For an uncontroversial evaluation of buoyancy effects, computations with gravity were also performed and the measured flame length was found to be the same as without
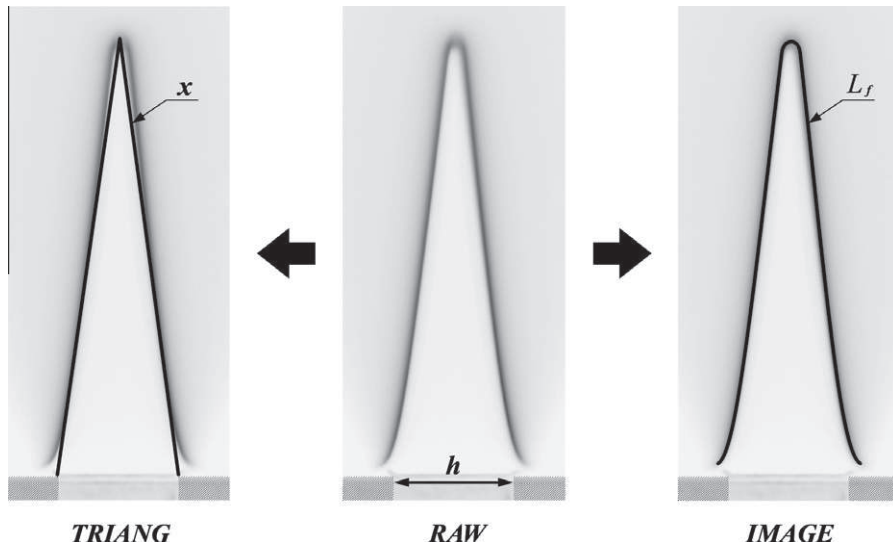

Fig. 4. Flame images obtained experimentally superimposed with the flame length detection method (bold line). Center: raw image. Left: TRIANG method (a triangle is fitted on the flame). Right: image processing is used to measure the flame length L_f.

gravity even though the burnt gases mix differently downstream the flame front with and without gravity.

Of course, the measurement of the flame length L_f can also be affected by other uncertainties and great care was used to identify the isoline of the images which tracks the reaction-rate zone. In a first step, however, we will concentrate on the systematic errors (a) to (c) and see if these errors are significant and must be accounted for. If they are, our objective is to see whether Eq. (1) can be corrected to use $\bar{s}_L$ as a measure of s_L^0. To do this, the ratio $s_L^0/\bar{s}_L$ is measured in the DNS and the correction factor for systematic errors (a) to (c) is introduced as a factor η_1:

$$\eta_1 = \frac{s_L^0}{\bar{s}_L} \tag{2}$$

The three-dimensional effects cannot be obtained from the two-dimensional DNS and will be quantified using velocity field measurements and introduced through a factor $\eta_2 = U/U_b$ so that a proper evaluation of the laminar flame speed will be:

$$s_L^0 = \bar{s}_L \eta_1 \eta_2 = \frac{Uh}{L_f} \eta_1 \eta_2 \tag{3}$$

4. Numerical tools

Two codes will be used for this study:

- a laminar flame code (COSILAB) which provides the flame speed for any chemical scheme. Here the GRI-Mech 3.0 scheme [37] will be used for CH_4–air flames,
- a two-dimensional DNS code which is used to compute the slot-burner configuration of Fig. 1 with a reduced scheme called 2SCM2. Using GRI-Mech 3.0 in such a code is possible today [46–48] but would be expensive and is not needed: the flame is mainly controlled by heat losses to the flame base and by the flame response to stretch.

The two-step scheme 2SCM2 [40] takes into account six species (CH_4, O_2, CO_2, CO, H_2O and N_2) and two reactions:

$$CH_4 + \frac{3}{2}O_2 \rightarrow CO + 2H_2O \tag{4}$$

$$CO + \frac{1}{2}O_2 \leftrightarrow CO_2 \tag{5}$$

The first reaction (4) is irreversible whereas the second one (5) is reversible and leads to an equilibrium between CO and CO_2 in the burnt gases. The rates of reaction (4) and (5) are respectively given by:

$$q_1 = A_1 \left(\frac{\rho Y_{CH_4}}{W_{CH_4}}\right)^{n_1^{CH_4}} \left(\frac{\rho Y_{O_2}}{W_{O_2}}\right)^{n_1^{O_2}} \exp\left(-\frac{E_{a1}}{RT}\right) \tag{6}$$

$$q_2 = A_2 \left[\left(\frac{\rho Y_{CO}}{W_{CO}}\right)^{n_2^{CO}} \left(\frac{\rho Y_{O_2}}{W_{O_2}}\right)^{n_2^{O_2}} - \left(\frac{\rho Y_{CO_2}}{W_{CO_2}}\right)^{n_2^{CO_2}}\right] \exp\left(-\frac{E_{a2}}{RT}\right) \tag{7}$$

where the parameters are provided in Table 1. This scheme was validated vs. GRI-Mech 3.0 for laminar flame speed and burnt gases adiabatic temperature since stretch may influence the local consumption speed in the slot burner case, additional validations were carried out: Fig. 5 compares computations with COSILAB of 2SCM2 and GRI-Mech 3.0 in the opposed-jet flame configuration for various jet velocities. It is clear that the reduced schemes performs well, matching GRI-Mech 3.0 with a maximum deviation of 4%. Note that the Lewis number of methane and air remain close to unity so that differential diffusion effects, which are accounted for in the DNS, remain limited. The transport coefficients used for 2SCM2 are sum-

Table 1
Rate constants for the 2SCM2 scheme used in the two-dimensional DNS code: the activation energies are in cal/moles and the preexponential constants in cgs units.

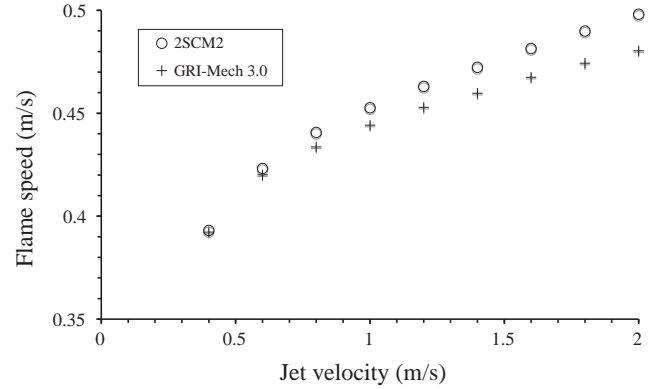| A_1	$n_1^{CH_4}$	$n_1^{O_2}$	E_{a1}	A_2	n_2^{CO}	$n_2^{O_2}$	$n_2^{CO_2}$	E_{a2}
210^{15}	0.9	1.1	34,500	210^9	1	0.5	1	12,000

Fig. 5. Validation of the reduced scheme 2SCM2 vs. GRI-Mech 3.0 for the influence of stretch on the flame speed. Numerical simulations in the opposed-jet configuration.

marized in Table 2. The Prandtl number is set to 0.68. The extension of this study to hydrogen flames is addressed in Section 8.

Using both tools together brings new insight into the flame structure. COSILAB is useful to provide the most precise estimate of the premixed laminar flame speed s_L^0 using the most recent chemical scheme (GRI-Mech 3.0) but cannot be used simply in a multidimensional configuration. The DNS code on the other hand, can compute the exact geometry of the experiment using unstructured meshes. DNS captures the quenched zone near the lips of the slot where temperature is imposed. It also includes strain and curvature effects present in the real configuration.

5. Effects of stretch and heat losses using DNS: determination of η_1

In a first step, the DNS was run for $\phi = 0.8$ and $\phi = 1$. For these cases, the flame speeds obtained in a one-dimensional configuration using the same mesh are $s_L^0(2SCM2) = 0.27$ m/s and 0.372 m/s, respectively. The DNS results for the stoichiometric flame are displayed on Fig. 6 which also shows a view of the whole computational domain and the unstructured mesh. The unstructured grid starts in the plenum feeding the slot and ends in the atmosphere, far from the flame zone to avoid effects of boundary conditions. The flame position can be isolated from the DNS data and various statistics can be gathered as a function of the flame abscissa. The simplest analysis consists in applying to the DNS data, the same methods used for the experiment (TRIANG and IMAGE). To do this, a fuel mass-fraction isoline is used to identify the flame front: $Y_f = 0.007$ for $\phi = 0.8$ and 0.012 for $\phi = 1$. This line corresponds almost exactly to the location of maximum reaction rate in both cases. For the IMAGE method, the flame length is defined as the length of the mass-fraction isolevel where the reaction rate is larger than half its maximum value: this criterion was devised to exclude the flame base region where the flame is quenched. Table 3 summarizes the flame speeds measured

Table 2
Schmidt numbers used in the two-dimensional DNS code.

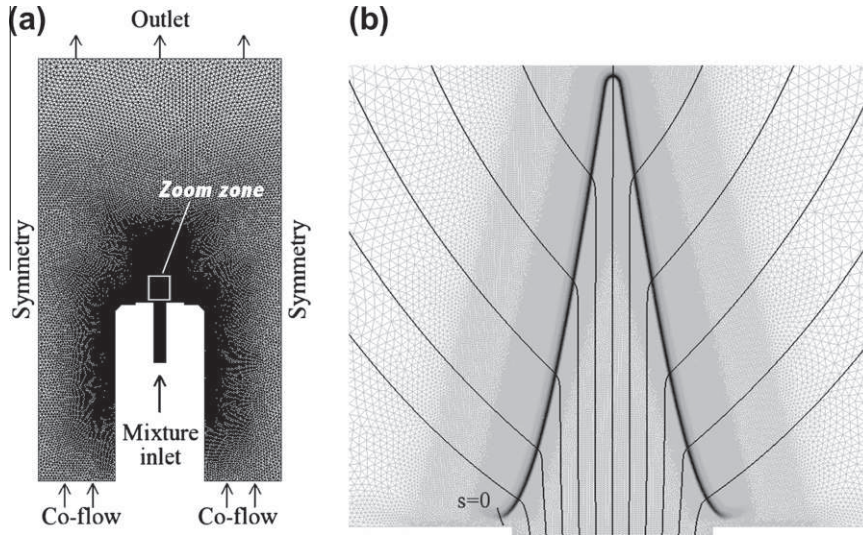| CH_4	CO_2	CO	O_2	H_2O	N_2
0.68	0.98	0.76	0.76	0.6	0.75

Fig. 6. (a) Total computational domain and mesh. (b) Zoom on white rectangle in image (a) on flame: streamlines, mesh (triangles) and reaction rate field (gray levels).

Table 3
Summary of flame speed values obtained by post processing DNS fields and comparison with the unstretched laminar flame speed s_L^0. The same chemical scheme (2SCM2) is used for all computations.

Case	s_L^0(2SCM2)	$\bar{s}_L$(TRIANG)	η_1(TRIANG)	$\bar{s}_L$(IMAGE)	η_1(IMAGE)
$\phi = 0.8$	0.270	0.266	1.016	0.2695	1.0014
$\phi = 1$	0.372	0.368	1.011	0.370	1.007

using both methods TRIANG and IMAGE (Fig. 4) and compares them to s_L^0(2SCM2) for an equivalence ratio of 0.8 and 1. The ratio η_1 between s_L^0(2SCM2) and $\bar{s}_L$ is always larger than unity indicating that the average flame speed underestimates the true laminar flame speed. However, η_1 is always close to unity and errors are smaller than 1.5% for both TRIAN and IMAGE methods, showing that the slot-burner technique is very accurate in these conditions. A correction factor η_1 of 1.01 will be retained for the TRIANG method and 1.005 for the IMAGE method.

The previous DNS results provide useful global information to correct measurements but DNS data can also be used to analyse the local flame structure and verify for example the variations of the flame speed and flow along the flame front abscissa s, from the flame base (s = 0) to the flame tip (s = L_f/2 see Fig. 4). Important quantities for laminar premixed flames are:

- The displacement speed $s_d = (\vec{w} - \vec{u}) \cdot \vec{n}$ where $\vec{w}$ is the absolute velocity of the flame front (zero in this case), $\vec{u}$ is the flow speed and $\vec{n}$ is the flame normal (computed as $\vec{n} = \vec{\nabla} \cdot T/|\vec{\nabla} \cdot T|$). The local displacement speed is not a direct measure of the laminar flame speed. A commonly used estimation of the local flame speed using s_d is [8]: $s_c^{from\,s_d} = s_d T/T_0$ where T is the local flame temperature and T_0 the fresh gas temperature.
- The true consumption speed s_c which is given by $s_c = (\int \dot{\omega}_F dn)/\rho_0 Y_F^0$ where $\dot{\omega}_F$ is the fuel reaction rate, ρ_0 is the fresh gas density and Y_F^0 is the fuel mass fraction in the fresh gases. The integral over $\dot{\omega}_F$ is performed along the local flame normal $\vec{n}$.
- The flame strain term which is the velocity gradient in the flame plane: $\partial u_t/\partial t$ where t is the coordinate in the plane tangent to the flame (i.e. $\vec{n} \cdot \vec{t} = 0$) and $u_t = \vec{u} \cdot \vec{t}$.
- The flame curvature $\mathscr{R}$ which can be obtained from the derivative of the temperature field for example: $\mathscr{R} = \vec{\nabla} \cdot \vec{n}$.
- The flame stretch κ which is the main parameter controlling the flame structure [36]: $\kappa = \partial u_t/\partial t + s_d/\mathscr{R}$

All these quantities have been measured on the 2D flame of Fig. 6 computed by DNS. Figure 7 displays profiles of strain, curvature and stretch along the flame abscissa. All terms are normalized by the inverse characteristic flame time s_L^0/δ_L^0: significant effects are expected only when these reduced values (similar to Karlovitz numbers) reach values close to unity. Note that the flame is stretched on its sides (positive stretch) but compressed at its tip (stretch is negative) as expected. Figure 7a shows that the overall stretch is very small everywhere along this flame. Effects of strain or curvature are very limited and the flame behaves as if it was unstretched. At the flame tip, the stretch becomes very negative leading to Karlovitz numbers of the order of −10 but over a very limited region.

Fig. 7b displays the two consumption speeds which can be extracted from the DNS: s_c and $s_c^{from\,s_d}$. The effect of heat losses can be observed for small values of the flame abscissa: at the flame base (s = 0), the consumption speed s_c is lower but goes up to s_L^0 rapidly. s_c is then almost constant, explaining why the averaged value of the flame speed is close to s_L^0. Strong changes in consumption speeds are observed only at the flame tip ($s/\delta_L^0 = 60$) where the compressed front leads to a higher reaction rate. Finally, note that even though s_c and $s_c^{from\,s_d}$ are close in the unstretched region, they differ in the quenched zone (at the flame base) and in the curved zone (at the flame tip) showing that the approximation used for $s_c^{from\,s_d}$ is valid only for simple flames and should not be used in more complicated situations.

6. Evaluation of three-dimensional corrections (η_2)

Another error factor comes from the fact that the flow issuing from the slot is not perfectly two-dimensional. At the two extremities of the slot ($y = 0$ and $y = L$ in Fig. 1), the velocity goes to zero so that the flow has to accelerate in the center of the channel where the mean velocity U (averaged in the transverse direction x in Fig. 1) is larger than U_b, the speed averaged over the whole slot. This increased velocity makes the flame slightly longer in the mid-section of the slot, where the flame length is measured and leads to a a systematic bias $\eta_2 = U/U_b$ in the evaluation of the flame speed by Eq. (1).

Assuming that the flow is established at the duct outlet (ie that the feeding duct is infinitely long), the correction factor η_2 can be estimated analytically using for example the results of Tatsumi and Yoshimura [49] who computed the established velocity profile
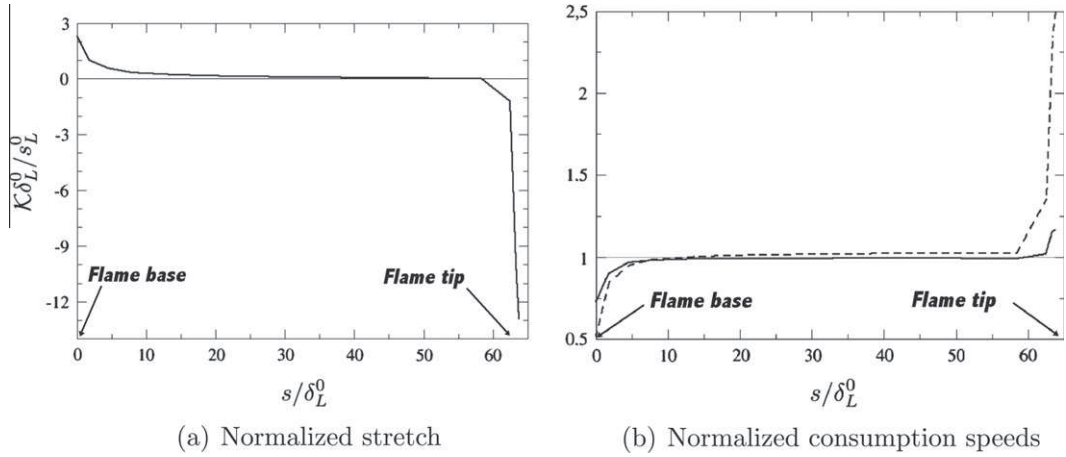
(a) Normalized stretch

(b) Normalized consumption speeds

Fig. 7. DNS results. Left: stretch (scaled by inverse characteristic flame time s_L^0/δ_L^0) vs. flame abscissa (scaled by flame thickness δ_L^0). Right: consumption speed s_c (solid line) and speed obtained from the displacement speed $s_c^{from\,s_d} = s_d T/T_0$ (dashed line) vs. normalized flame abscissa. Speeds normalized by the laminar flame speed s_L^0 (2SCM2).

for a laminar flow in a rectangular duct (which is a good approximation for the present case). These authors solved the Poisson equation for the axial velocity field in a rectangular duct using Legendre polynomia. They show that transverse velocity profiles ($u(x,y)$ at fixed y) remain parabolic and they provide a simple fit (valid for a slot aspect ratio $\alpha \geqslant 3$) linking the maximum velocity in the channel, $u(x=0,y=L/2)$, as a function of the bulk velocity U_b and the aspect ratio α of the duct: $U_b/u(x=0,y=L/2) = 2/3 - 0.4201/\alpha$. From this relation, the η_2 factor can be obtained using $U = 2/3 \times u(x=0,y=L/2)$:

$$\eta_2^{ana} = \frac{1}{1 - 0.6301/\alpha} \qquad (8)$$

Here, the aspect ratio α is 10 so that η_2^{ana} is 1.067.

To verify this evaluation of η_2, Pitot tube measurements were also performed on the experiment to evaluate the axial velocity along two lines: $y = L/2$ and $x = 0$ (cf. Fig. 1). As expected, two boundary layers are observed at the extremities $y = 0$ and $y = L$ of the slot (Fig. 8b) but the axial velocity profile in the transverse direction (Fig. 8a) is not perfectly parabolic, indicating that the flow is not fully established. The correction factor η_2 can be evaluated using the velocity measurements of Fig. 8b. For a very long slot (i.e. large α), the velocity profile at the center of the slot ($y = L/2$) is given by the Poiseuille solution:

$$u^{Poi}(x) = \frac{3}{2} U_b \left(1 - \left(\frac{x}{l} \right)^2 \right) \qquad (9)$$

For a finite A slot like in the present experiment, the Pitot tube measurements provide the axial velocity profile (Fig. 8a) and the correction factor η_2 is simply expressed as
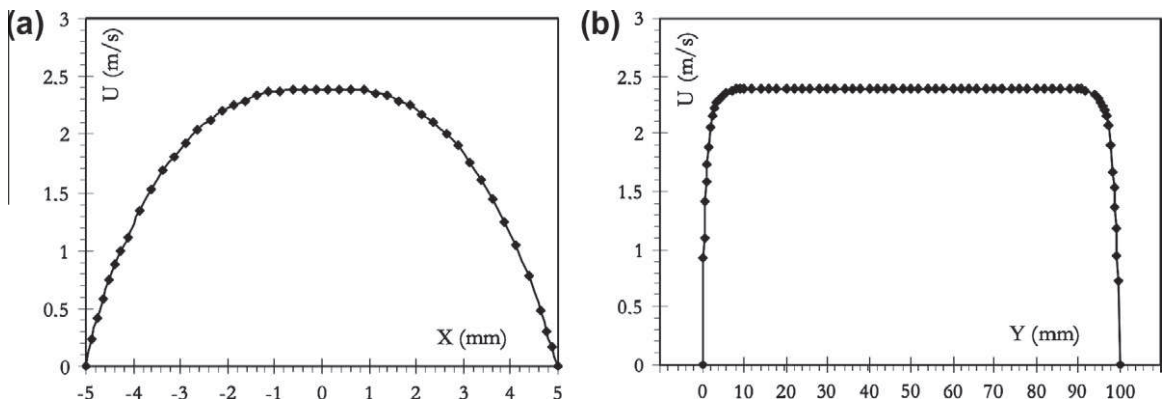
$$\eta_2^{exp} = \frac{\int_{-h/2}^{h/2} u(x, y = L/2) dx}{\int_{-h/2}^{h/2} u^{Poi}(x) dx} \qquad (10)$$

This evaluation yields $\eta_2^{exp} = 1.054$, which is close to the value obtained analytically ($\eta_2^{ana} = 1.067$ using Eq. (8). The experimental value $\eta_2 = 1.054$ was kept for the evaluation of s_L^0.

7. Application

Sections 5 and 6 can be summarized as follows: in the slot burner of Fig. 1, the unstretched laminar flame speed s_L^0 can be obtained from the averaged flame speed $\bar{s}_L$ in a transverse plane by correcting it by two factors η_1 and η_2: η_1 integrates the effect of quenching at the flame base, strain and curvature effects. It is a small correction, estimated from a two-dimensional DNS as $\eta_1 = 1.010$ for method TRIANG and 1.005 for method IMAGE. η_2 is due to boundary effects at each extremity of the slot which lead to a flow acceleration at the center of the slot where the flame shape is visualized and used to measure $\bar{s}_L$. This factor depends only on the aspect ratio of the rectangular duct and is of the order of $\eta_2 = 1.054$ for the present channel.

7.1. Methane/air flames

The final result $s_L^0 = \eta_1 \eta_2 \bar{s}_L$ is now used to post process experimental results for a methane/air flame at atmospheric pressure and temperature ($T_0 = 300$ K). The method used to measure the flame length is method IMAGE but method TRIANG leads to almost identical values. Flame speed (s_L^0) measurements are compared

Fig. 8. Axial velocity profiles obtained experimentally. (a) Transverse direction: $u(x, y = L/2)$; (b) longitudinal direction: $u(x = 0, y)$.

over a range of equivalence ratios with various other results: the numerical output of COSILAB in the same conditions is used as a reference but other experimental data are also introduced for comparison [12,50–52,28,53]. Figure 9 displays flame speed values from $\phi = 0.8$ to 1.2. The only numerical result in Fig. 9 is the COSILAB data obtained with GRI-Mech 3.0. Measurements were performed in the slot-burner set-up using an outlet bulk velocity $U_b = 1.9$ m/s. The effect of this velocity was verified by changing U_b from 1.2 to 1.9 m/s: such changes lead to variations in s_L^0 smaller than 0.3%. The present measurements agree well with COSILAB results. They are slightly higher than other experiments for lean flames (except for the data of Gu et al. [51]) and slightly below them for rich flames (except for the data of Halter et al. [54]). Considering the error bars on all flame-speed measurements (see for example a summary of measured values for methane/air flames in [28]), it is difficult to determine which method is the best but the present one obviously gives reasonable results and matches GRI-Mech 3.0 results very well.

7.2. Methane/air flames with water vapor

This section presents an application of the slot-burner method to measure flame speeds of methane/air mixtures where the air contains water vapor. In most practical applications of combustion in air, significant amount of water vapor may be present in the air stream, either because of natural atmospheric conditions or through intentional water addition. For example, in gas turbines water is added to lower emission levels; in piston engines when Exhaust Gas Recirculation (EGR) is used, water present in the combustion products modifies the flame speed by changing the heat capacity of the mixture, but also its kinetics. Measuring these effects is of interest and the slot burner methodology was applied to the combustion of methane in air containing water vapor. Since the Lewis number of water vapor is close to unity, the local effects of stretch and curvature are expected to match those of the methane/dry-air flame. Consequently, the correction factor η_1 derived in Section 5 is retained. The factor η_2 solely depending on the burner geometry is also kept constant. The water-vapor content is quantified by the specific humidity s_H, defined as the ratio of the mass of vapor to the total mass of humid air (air plus water). At a given temperature, the specific humidity is bounded by the saturation of water in air: typically, at $T = 300$ K, the saturation specific humidity is $s_H^{sat} = 21.8$ g/kg and at $T = 330$ K, $s_H^{sat} = 112$ g/kg. The measurements of laminar flame speed s_L^0 at stoichiometry for three fresh-gases temperature are presented in Fig. 10, together with numerical simulations using COSILAB and GRI-Mech 3.0. The two lower temperatures correspond to operating conditions of an air-breathing engine in standard to extreme conditions. Because saturation occurs for smaller s_H values at lower temperatures, only
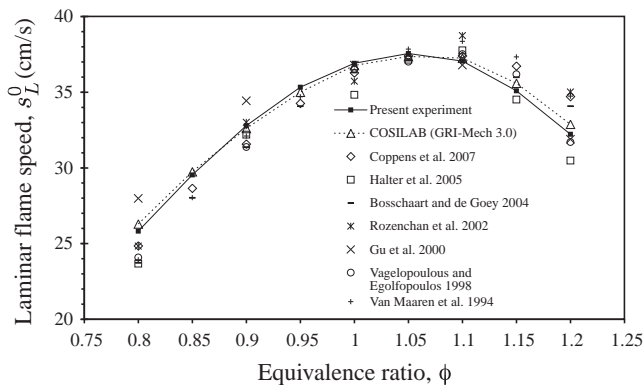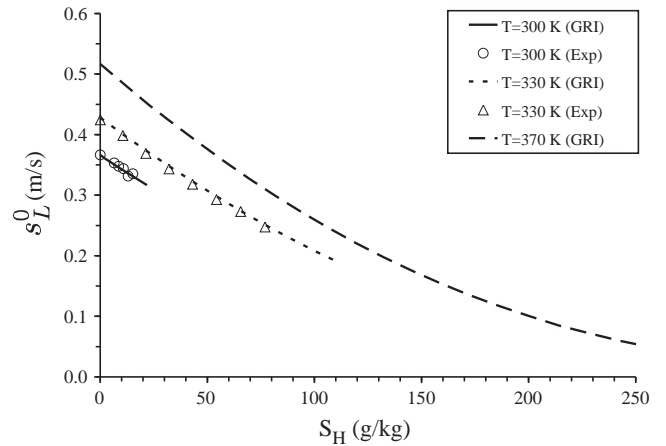

Fig. 10. Laminar flame speed s_L^0 vs. specific humidity s_H at 1 bar for a stoichiometric flame. Symbols are experimental results, lines correspond to simulations with COSILAB and GRI-Mech 3.0. Simulations at 300 K and 330 K are conducted up to the saturation point of water vapor in air.

a limited amount of water can be added to air at 300 K and the flame speed is mildly affected: s_L^0 is reduced by less than 15%. However, at 330 K s_L^0 can be divided by two, which may have a significant impact on the operation of the engine. For these two conditions, the measurements closely match the numerical simulations of COSILAB. For engines that may have a much higher inlet temperature together with direct water addition or EGR, a numerical simulation at 370 K shows that the flame speed can be reduced by 90%. These effects are important and must be incorporated in models used for combustion in piston engines and gas turbines.

8. Extension to other flames and limitations

The previous sections have shown that the slot burner was a reasonably accurate and inexpensive technique to measure flame speeds for methane/air mixtures. Similar methods are routinely used in the literature to measure flame speeds and an interesting question that came out during this work is the validity of the approach in a more general framework: can this method be used for all mixtures? The answer is negative because of multiple factors:

1. Very slow flames will be submitted to buoyancy effects.
2. Slot flames are also known to be highly unstable, exhibiting strong pulsations. In most cases, these pulsations are due to acoustic coupling mechanisms between the flame and the plenum [55–57].
3. Flames with non-unity Lewis number are strongly affected by preferential diffusion where the reaction zone is curved. For a slot flame, both the tip and the shoulder are curved potentially affecting the average flame speed and leading to non-unity values for the correction factor η_1 defined in Eq. (2). This effect is actually even worse for conical flames because these are curved everywhere.
4. The method works only for steady flames: any instability or fluctuation will affect precision. Thermodiffusive effects or, in the case of very fast flames, turbulence might lead to oscillating flames and make flame-speed measurements impossible.
5. Fast flames may flashback in the injection tube, especially if the flame is submitted to acoustic oscillations.

During this work, the influence of some of these effects was investigated either experimentally or using simulations.

Fig. 9. Laminar flame speed s_L^0 vs. equivalence ratio ϕ at 300 K and 1 bar.

1. Simulations with gravity (and even negative gravity corresponding to an upside-down flame) were performed for the methane/air flame at $\phi = 0.8$. The hot gases plume was affected by gravity but the length of the reaction zone was not. This may change for very slow flames, especially near the flammability limits.

2. Strong oscillations at the frequency of the Helmholtz mode of the plenum (around 60 Hz) were present when the apparatus was first fired. Measurements were impossible with such instabilities. However, the oscillations were easily damped by increasing the acoustic dissipation in the system: here, using a longer exhaust pipe (therefore increasing the dissipation of the Helmholtz mode) was sufficient to damp all acoustic activity and ensure that the flame remains perfectly stable.

3. The effect of non-unity Lewis number was thought to be critical so it was decided to conduct simulations of hydrogen/air flames. A DNS at 300 K and 1 bar was performed with a complex chemical scheme (six species: H_2, O_2, OH, H, O, H_2O) and seven reactions [58]. The slot width, h, is the same as for the methane flames. Two equivalence ratios were tested: $\phi = 0.6$ and 0.8. The objective is the determination of the correction factor η_1 which was shown to be very close to unity for methane/air flames. Incidentally, because hydrogen flames have larger flame speed, the fresh-gases velocity is significantly larger (for a flame of roughly 2 cm height, $U = 3.8$ m/s at $\phi = 0.6$ and $U = 6$ m/s at $\phi = 0.8$) so that these simulations also address the issue of flame steadiness for fast flames. For these hydrogen/air flames, the tip of the flames kept oscillating (Fig. 11), leading to variations of η_1. At $\phi = 0.8$ the correction factor oscillated between -1.3% and $+1.4\%$ and at $\phi = 0.6$, between -1.6% and -0.5%. This raises doubts on the applicability of the technique for such flames. Furthermore, flame tip opening was observed at $\phi = 0.6$ (Fig. 11a), which is consistent with the negative average correction factor around -1%.

4. The simulation of the hydrogen flame at $\phi = 0.8$ ultimately failed because of flashback: one shoulder of the flame would enter the inlet tube and propagate upstream.

Slot burner experimental measurements of hydrogen/air flames have been reported [59,60] and obviously, there are methods to control flashback, average small oscillations of the flame tip or extra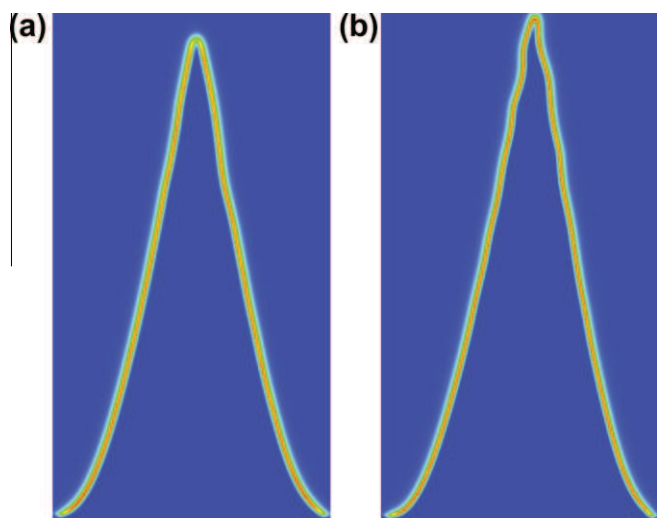polate the flame position when the tip is opening but there is little doubt that the accuracy of the technique becomes questionable in such flames.

9. Conclusion

Two-dimensional slot burners are an interesting configuration to measure laminar flame speeds because they allow to generate an uncurved, unstrained, steady flame over a large region. In this paper, sources of errors in the measurement of laminar flame speeds using such a setup have been evaluated using a combination of experimental and numerical (1D and 2D DNS) tools for a methane/air flame. A global analysis of two-dimensional DNS data show that the corrections due to quenching at the flame base, strain on the flame sides and curvature at the tip are almost negligible (of the order of 1%). Local analysis of DNS results confirm that most of the flame sheet is uncurved and unstrained, making it a proper prototype for flame-speed measurements. Results also prove that for methane/air flames, the only significant correction needed in a 2D slot-burner set-up comes from the finite aspect ratio of the slot ($\alpha = 10$ in the present study) used to stabilize the flame: it leads to flow acceleration in the mid-part of the slot and a correction of the order of 5% for the present configuration. If the slot feeding the flame is sufficiently long, a comparison with experimental velocity measurements showed that the analytical expression of Tatsumi and Yoshimura [49] provides a very good evaluation of this correction factor. Using these corrections, the methane/air flame speed measured in the experiment matches the value computed by COSILAB and the GRI-Mech 3.0 scheme as well as most other experimental data for equivalence ratios going from 0.8 to 1.2. The methodology was also used to study the influence of water vapor addition on flame propagation. The results match the predictions of numerical simulations with GRI-Mech 3.0 and show that water addition has a first-order effect on premixed laminar flame speeds. Even though present results show that the slot burner is well adapted to measure methane/air flame speeds in a certain range and for certain fuels, it can not be extended without significant difficulties to measure all flame speeds for all fuels: DNS performed for H_2/air fuels revealed much larger error margins for these fast, thermodiffusively unstable flames. In the quest for the ultimate method to measure flame speeds in all cases, the slot burner will not be a good candidate. It is however a good method to measure flame speeds for fuels like methane and to evaluate the effects of limited variations in composition on flame speeds (adding H_2, H_2O or bio-fuels for example).

Fig. 11. Heat release fields in the DNS of hydrogen/air flames: (a) $\phi = 0.6$ and (b) $\phi = 0.8$. The inlet temperature is 300 K and the inlet velocity is modulated so that the two flames have a height around 2 cm.

References

[1] P. Laffitte, La propagation des flammes dans les mélanges gazeux, Hermann et Cie, Actualités scientifiques et industrielles, PARIS, 1939.
[2] H. Le Chatelier, Lecons sur le carbone, la combustion, les lois chimiques, Hermann, 1907.
[3] R.V. Wheeler, J. Chem. Soc. 115 (1919) 81.
[4] E. Mallard, H. Le Chatelier, Ann. Min. 4 (1883) 274.
[5] K.N.C. Bray, M. Champion, P.A. Libby, in: R. Borghi, S. Murthy (Eds.), Turbulent Reactive Flows, vol. 40, Lecture Notes in Engineering, Springer-Verlag, 1989, pp. 541–563.
[6] N. Peters, Turbulent Combustion, Cambridge University Press, 2001.
[7] D. Veynante, L. Vervisch, Prog. Energy Comb. Sci. 28 (2002) 193–266.
[8] T. Poinsot, D. Veynante, Theoretical and Numerical Combustion, second ed., R.T. Edwards, 2005.
[9] S.B. Pope, Ann. Rev. Fluid Mech. (1994) 23–63.
[10] S. Richard, O. Colin, O. Vermorel, A. Benkenida, C. Angelberger, D. Veynante, Proc. Combust. Inst. 31 (2007) 3059–3066.
[11] E. Mallard, H. Le Chatelier, Comptes rendus de l'Academie des Sciences, Paris 93 (1881) 145.
[12] C.M. Vagelopoulos, F. Egolfopoulos, in: 27th Symp. (Int.) on Combustion, The Combustion Institute, Pittsburgh, 1998, pp. 513–519.
[13] F. Egolfopoulos, C.K. Law, in: 25th Symp. (Int.) on Combustion, The Combustion Institute, Pittsburgh, 1994, pp. 1341–1347.
[14] C.K. Law, S. Ishizuka, M. Mizomoto, in: 18th Symp. (Int.) on Combustion, The Combustion Institute, Pittsburgh, Waterloo, Canada, 1981, pp. 1791–1798.

[15] V. Giovangigli, M. Smooke, J. Comput. Phys. 68 (2) (1987) 327–345.
[16] S. Ishizuka, C.K. Law, in: 19th Symp. (Int.) on Combustion, The Combustion Institute, Pittsburgh, 1982, pp. 327–335.
[17] R.V. Wheeler, J. Chem. Soc. 113 (1918) 840.
[18] O. Ellis, R.V. Wheeler, J. Chem. Soc. (1927) 153–158.
[19] M.I. Hassan, K.T. Aung, G.M. Faeth, Combust. Flame 115 (4) (1998) 539–550.
[20] D.R. Dowdy, D.B. Smith, S.C. Taylor, in: 23rd Symp. (Int.) on Combustion, The Combustion Institute, Pittsburgh, 1990, pp. 325–332.
[21] D. Bradley, P.H. Gaskell, X.J. Gu, Combust. Flame 104 (1/2) (1996) 176–198.
[22] K.T. Aung, M.I. Hassan, G.M. Faeth, Combust. Flame 112 (1) (1998) 1–15.
[23] R.G. Abdel-Gayed, D. Bradley, M.N. Hamid, M. Lawes, Proc. Combust. Inst. 20 (1984) 505–512.
[24] B. Renou, A. Mura, E. Samson, A. Boukhalfa, Combust. Sci. Technol. 174 (4) (2002) 143–179.
[25] S. Shy, S. Yang, W. Lin, R. Su, Combust. Flame 143 (1–2) (2005) 106–118.
[26] J. Botha, D. Spalding, Proc. R. Soc. Lond. A 225 (1954) 71–96.
[27] K. Bosschaart, L. de Goey, Combust. Flame 132 (2003) 170–180.
[28] K. Bosschaart, L. de Goey, Combust. Flame 136 (2004) 261–269.
[29] M. Remie, M. Cremers, K. Schreel, L. de Goey, Combust. Flame 147 (2006) 163–170.
[30] G. Garcia-Soriano, F.J. Higuera, J.L. Castillo, P.L. Garcia-Ybarra, in: Proc. of the European Combustion Meeting, Vienna, Austria, 2009.
[31] G.I. Sivashinsky, Combust. Sci. Technol. 15 (1977) 137–146.
[32] P. Clavin, Proc. Combust. Inst. 28 (2000) 569–586.
[33] T. Poinsot, Combust. Flame 113 (1998) 279–284.
[34] R.A. Strehlow, L.D. Savage, Combust. Flame 31 (1978) 209.
[35] S.M. Candel, T. Poinsot, Combust. Sci. Technol. 70 (1990) 1–15.
[36] F.A. Williams, Combustion Theory, Benjamin Cummings, Menlo Park, CA, 1985.
[37] M. Frenklach, H. Wang, M. Goldenberg, G.P. Smith, D.M. Golden, C.T. Bowman, R.K. Hanson, W.C. Gardiner, V. Lissianki, GRI-Mech: An Optimized Detailed Chemical Reaction Mechanism for Methane Combustion, Tech. Rep. GRI-Report GRI-95/0058, Gas Research Institute, 1995.
[38] A. Kaufmann, F. Nicoud, T. Poinsot, Combust. Flame 131 (2002) 371–385.
[39] K. Truffin, T. Poinsot, Combust. Flame 142 (4) (2005) 388–400.
[40] L. Selle, G. Lartigue, T. Poinsot, R. Koch, K.-U. Schildmacher, W. Krebs, B. Prade, P. Kaufmann, D. Veynante, Combust. Flame 137 (4) (2004) 489–505.
[41] L. Ubbelohde, M. Hofsass, J. Gasbeleucht 56 (1225 and 1253) (1913).
[42] L. Ubbelohde, E. Koelliker, J. Gasbeleucht 59 (49, 65, 82 and 98) (1919).
[43] J. Corsiglia, American Gas Association Monthly 13 (1931) 437.
[44] B. Bédat, R.K. Cheng, Combust. Flame 107 (1–2) (1996) 13–26.
[45] L. Muniz, M.G. Mungal, Combust. Flame 126 (1–2) (2001) 1402–1420.
[46] M.D. Smooke, P. Lin, J. Lam, M.B. Long, in: 23rd Symp. (Int.) on Combustion, The Combustion Institute, Pittsburgh, 1990, pp. 575–582.
[47] R. Sankaran, E. Hawkes, J. Chen, T. Lu, C.K. Law, Proc. Combust. Inst. 31 (2007) 1291–1298.
[48] J. Bell, M. Day, J. Grcar, M. Lijewskia, J.F. Driscoll, S. Filatyev, Proc. Combust. Inst. 31 (2007) 1299–1307.
[49] T. Tatsumi, T. Yoshimura, J. Fluid Mech. 212 (1990) 437–449.
[50] A. Van Maaren, D.S. Thung, L.R.H. De Goey, Combust. Sci. Technol. 96 (4) (1994) 327–344.
[51] X.J. Gu, M.Z. Haq, M. Lawes, R. Woolley, Combust. Flame 121 (2000) 41–58.
[52] G. Rozenchan, D. Zhu, C. Law, S. Tse, Proc. Combust. Inst. (29) (2002) 1461–1469.
[53] F. Coppens, J. De Ruyck, A. Konnov, Exp. Therm. Fluid Sci. (31) (2007) 437–444.
[54] F. Halter, C. Chauveau, N. Djebaili-Chaumeix, I. Gokalp, Proc. Combust. Inst. (30) (2005) 201–208.
[55] T. Lieuwen, J. Fluid Mech. 435 (2001) 289–303.
[56] N. Noiray, D. Durox, T. Schuller, S. Candel, Combust. Flame 145 (3) (2006) 435–446.
[57] D. Durox, T. Schuller, N. Noiray, A. Birbaud, S. Candel, Combust. Flame 155 (3) (2008) 416–429.
[58] G. Lacaze, B. Cuenot, T.J. Poinsot, M. Oschwald, Combust. Flame 156 (6) (2009) 1166–1180.
[59] J. Natarajan, T. Lieuwen, J. Seitzman, Combust. Flame 151 (1–2) (2007) 104–119.
[60] C. Dong, Q. Zhou, Q. Zhao, Y. Zhang, T. Xu, S. Hui, Fuel 88 (1858–1863).